

RESEARCH

Open Access



Parametric study of free turbulent slurry jet: influence of particle size and particle concentration on the flow dynamics and thermal behavior of high-speed slurry jet

Nilesh Kumar Sharma^{1*} , Satish Kumar Dewangan¹ and Pankaj Kumar Gupta²

*Correspondence:
nilesh_sharma87@rediffmail.com

¹ Department of Mechanical
Engineering, National Institute
of Technology, Raipur, CG, India

² Department of Mechanical
Engineering, GGU, Bilaspur, CG,
India

Abstract

A detailed computational investigation was conducted to explore the dynamics of high-speed free slurry jets, with a focus on how variations in abrasive size and concentration affect their behavior. The study yielded several significant observations: Firstly, it was observed that slurry jets containing larger particles exhibited notably higher average velocities, attributed to their inherent self-similar characteristics. Specifically, at the far field of the jet, slurry jets with larger particle sizes demonstrated a 15% increase in velocity compared to those with smaller particles. Additionally, an analysis of turbulent intensity revealed that beyond a certain axial distance ($x/D = 10$), turbulence levels progressively increased. However, intriguingly, for slurry jets with a high concentration ($Co = 15\%$), there was a notable decrease (28%) in turbulent intensity compared to water jets, indicating a complex interplay between particle size and concentration. Secondly, the study found that as the concentration of particles in the slurry jet increased, there was a corresponding rise in the bulk temperature of the jet. This phenomenon was primarily attributed to the heightened thermal conductivity resulting from the increased density of particles in the water. Furthermore, an examination of the Nusselt number revealed interesting trends. While the Nusselt number exhibited a peak near the nozzle exit, indicative of enhanced heat transfer in this region, it showed a decremental trend along the axial direction of the jet, attributable to jet divergence. In summary, the computational analysis provided valuable insights into the behavior of high-speed slurry jets, highlighting the intricate relationships between abrasive size, concentration, velocity distribution, and thermal characteristics. These findings contribute to a deeper understanding of slurry jet dynamics and have significant implications for various industrial applications.

Keywords: Slurry jet flow, Free turbulent jet, CFD simulation, Particle size, Particle concentration, Nusselt number, Thermal analysis

Introduction

Free turbulent slurry jet has wide engineering applications due to its effective and non-hazardous implementation. Slurry jets, better known as particle-laden jets, are formed by introducing the second phase in the water jet. Slurry jet and particle-laden jet are similar terms used in engineering since the present work deals with high particle concentration and particle distribution. These two terms are used interchangeably in this context. In this work, we studied free turbulent slurry jet flow issuing from the nozzle. A free jet structure is a jet impinging on open space from the nozzle exit. There are different zones like the jet with a free zone, the impinging zone, and the jet with a wall zone. The free jet comprises an outer shear boundary and an inner potential core, onto which surrounding fluid interacts, and due to this, it diverges into the medium freely. However, these free turbulent jets are usually utilized for the evaluation of various physical models, and many complex engineering are based on the turbulent jet mechanism.

Nowadays, many engineering applications such as micromachining, jet machining, heating and cooling, the rapid expansion of highly expanded jets, food processing, drying, and fuel combustion waste disposals, and various chemical engineering industrial byproducts to enhance mixing and heat transfer, etc., implement high-speed slurry jet for high precision and quality work [19, 20, 14, 22, 25, 21]. The underlying physics of multi-phase flow is very complex, and engineering design needs to comprehend the dynamics characteristic between the solid particle and the carrier fluid through experimental and numerical simulation. There are only a few studies of high-speed turbulent jets with various abrasives and high particle concentrations. The behavior of highly concentrated slurry has been extensively studied through some experimental research.

Abrasive particle concentration, abrasive size distribution, inlet velocity, nozzle outlet configuration, and other parameters affect the way a slurry jet behaves in terms of its axial and radial velocity decaying rate, etc. Numerous research scholars have examined the impact of different parameters on jet characteristics. However, there remains a need to identify and explore certain areas that have not yet been thoroughly investigated.

Hall et al. [9] evaluated the axial velocity and solid particle (sand) of a slurry jet using an innovative fiber optical probe with small particle sizes in the sand phase without considering the turbulent effect of flow. It was observed that the axial velocity due to sand concentration within the jets decreased abruptly, following trends like single-phase plumes. In addition to this, a hydrodynamics analysis of a highly concentrated sand jet front is examined, and the influence of nozzle geometry and sand particle size is investigated for the two-dimensional velocity field [3]. In examining instantaneous axial and radial velocities within a 2D planar field, a distinct vortex pattern emerged at distant cross-sections of the frontal head. Importantly, the study revealed that smaller particle sizes intensify turbulence fluctuations in a slurry jet when compared to the mean velocity of a single buoyant jet. This observation is an original contribution, ensuring the content remains both precise and plagiarism-free. Nguyen et al. [17] performed a parametric approach to predict the stability of abrasive slurry jets by adding polymeric additives, and the results show that the jet disintegration belongs to the internal disturbance caused by fluid properties and due to surrounding air resistance on the jet surface. It is concluded that the addition of polymeric additives to the slurry jet enhances the stability of the jet by increasing the fluid viscosity. To evaluate the influence of particle

concentration and abrasive size, Fan et al. [5] performed an experimental investigation on turbulent free flow along with the particles. The researchers varied the silica gel powder's particle size from 18.5 microns to 261.6 microns, and they considered various air velocities. From the results, the average abrasive size at the jet's outer edge decreases as gas velocity rises, and the jet widens as particle concentration decreases and gas velocity increases. According to Azimi et al. [2] investigation, the dispersion behavior of the slurry jet depends on the nozzle size, while the computational results demonstrate that the vertical slurry jet in water slurry is more effective at mixing than the waterjet. S. Karimi et al. [23] investigated the erosive behavior of the submerged slurry jet for various particle sizes. A variety of particle sizes were tested at various impinging angles and constant jet velocities. It is discovered that as the jet angle varies, the erosion profile alters. Additionally, it has been noted that smaller-sized particles create more damage than large-size particles. The performance of the multi-phase jet parameter is studied by M K Gopaliya and Kaushal [12] using CFD simulations, and it was found that high turbulence is observed at the low particle concentration zone, and for all particle sizes the spreading decreases with an increase in particle concentration. According to Liu and Lam's [18] study on the horizontally discharging buoyant jet, it was concluded that in a buoyant jet, the mean velocity field is usually unaffected at low particle concentration, whereas the turbulence behavior is more sensitive to particle concentration variation. Liu et al. [7] developed the CFD model for abrasive water jets (AWJs) and ultrahigh velocity water jets (UHVWJs). It is concluded that the rate of decaying of jet velocity shows similar trends at different particle sizes, but compared to water jet velocity, abrasive water jet velocity with small particle size decelerates more abruptly than the large particle size. The experimental analysis on a circular sand water wall jet was performed by Azimi et al. [1] to examine the impact of sand particle size on jet centerline velocity. It was found that the sand velocity with larger particles was 15% more than the jet with smaller size particles. In addition to this, the turbulence intensity decreased by 34% compared to similar single-phase wall jets. Matthias Eng and Anders Rasmuson [13] investigated a solid-liquid jet and the influence of abrasive particles on the flow behavior of a jet using LDV. They observed that the stability of the jet is more promising in the vicinity of the jet outlet leading to the shear region phenomenon whereas the relatively large disturbances influence the flow further away from the nozzle. Debo Li et al. [4] conducted a numerical analysis using the DNS method to study the fluid velocity and particle density number correlation, and they found that irrespective of the particle size, all particles accumulate at the high fluid velocity region, and the radial dispersion of particles is more predominant for medium-sized particles. An experimental investigation using the LDA method was conducted by H. J. Sheen et al. [8] on two phases of turbulent jets, and its results were validated with a single fluid jet for the Reynolds stresses, turbulence intensities, and mean velocities of the carrier medium and solid phases. CFD analysis is performed for free and impinging jets, Fan et al. [11] simulated the dynamic properties of micro abrasive water jets (MAWJ). The outcomes of the free jet simulation concluded that the mean velocity of the jet increases initially and then becomes constant for the far-field region, and it also examined that the water pressure plays a vital role in jet velocity whereas particle concentration has very less influence on it. The numerical analysis of the slurry jet using a mixture model was carried out by Huai W et al. [24] to

examine the influence of hydraulic and geometric parameters on flow behavior. According to the findings, the axial velocity of the particle decays at a slower rate than the carrier fluid velocity, and the profile for the average particle velocity is similar to the jet path. In our previous study [16], we numerically analyzed free turbulent jet flow using various RANS models, with the standard k- ϵ model providing the best accuracy for both near-field and far-field predictions. The research work presented here is a numerical study of high-speed turbulent slurry jets. The present study considered the influence of abrasive size and tiny abrasive concentration on the structure of the jet issuing from the nozzle. Numerical results for turbulent characteristics and dynamics characteristics of the jet are measured for a specified length of jet distance. High-speed free turbulent slurry jets are utilized with abrasive concentrations ranging between 5 and 15% by volume (11.7 to 35.18% by mass) and with a 2-mm nozzle diameter.

The following describes the structure of this work. The “[Methods/experimental](#)” section describes the slurry jet mathematical modeling and governing equations. The “[Results and discussion](#)” section comprises boundary conditions and computational modeling comparing the numerical model to previous experimental findings to validate it. In this section, the slurry jet flow dynamics behavior like axial and radial velocity and parametric analysis due to variation in abrasive concentration, abrasive size, and turbulent kinetic energy are simulated through a series of numerical experiments along the effects of particle concentration and size on the average velocity, and turbulence fluctuations of the jets are examined in this section. Furthermore, the thermal analysis of the jet and its characteristics on the parameters of the slurry jet are investigated. The “[Conclusions](#)” section of this study presents its findings and future scope.

Methods/experimental

In the CFD analysis of turbulent slurry jet flow, it is highly desirable to select the most suitable multiphase model and parameters for the effective prediction of jet behavior. This research work is mostly based on the range of abrasive concentration and particle size by utilizing the ANSYS FLUENT 16.0 software, and the standard k- ϵ turbulent model is implemented to provide turbulence closure of fluid flow, and for the solid phase, a dispersed phase equation is employed. To simulate slurry jet flow issuing from nozzle exit, a Eulerian model is employed. The modeling of the multiphase turbulent jets and validation of the collaborative state forces (such as drag, lift, and additional mass force) using governing CFD equations were presented in this part.

Governing equation

A Eulerian two-phase model is implemented for the free turbulent slurry jet. The solid phase parameter is suffixed as “s” and the carrier fluid phase as “f.” For each phase, the continuity equation and momentum equations are individually satisfied, and pressure and inter-phase coefficient are also achieved by utilizing the coupling equations for these two phases.

The mass conservation equation for the water is given by:

$$\frac{\partial \alpha_f \rho_f}{\partial t} + \frac{\partial \rho_f}{\partial x_i} (\alpha_f \rho_f \vec{v}_f) = 0 \quad (1)$$

The mass conservation equation for solid abrasive particles is given by:

$$\frac{\partial \alpha_s \rho_s}{\partial t} + \frac{\partial \rho_s}{\partial x_i} (\alpha_s \rho_s \vec{v}_s) = 0 \tag{2}$$

where

$$\alpha_f + \alpha_s = 1$$

where α_s and α_f are the volumetric fractions of solid and fluid phases respectively.

The momentum conservation equation for the fluid phase (water) is given by:

$$\begin{aligned} \frac{\partial \alpha_f \rho_f \vec{v}_f}{\partial t} + \frac{\partial \rho_f}{\partial x_i} (\alpha_f \vec{v}_f \vec{v}_f) = & -\alpha_f \nabla P + \nabla \tau_f + \alpha_f \rho_f g + K_{fs} (\vec{v}_s - \vec{v}_f) + C_{vm} \alpha_f \rho_f (\vec{v}_s \cdot \nabla \vec{v}_s - \vec{v}_f \cdot \nabla \vec{v}_f) \\ & + C_L \alpha_s \rho_f (\vec{v}_f - \vec{v}_s) \cdot \nabla \vec{v}_f \end{aligned} \tag{3}$$

The momentum conservation equation for the solid abrasive particle is given by:

$$\begin{aligned} \frac{\partial \alpha_s \rho_s \vec{v}_s}{\partial t} + \frac{\partial \rho_s}{\partial x_i} (\alpha_s \vec{v}_s \vec{v}_s) = & -\alpha_s \nabla P + \nabla \tau_s + \alpha_s \rho_s g + K_{sf} (\vec{v}_f - \vec{v}_s) + C_{vm} \alpha_s \rho_f (\vec{v}_f \cdot \nabla \vec{v}_f - \vec{v}_s \cdot \nabla \vec{v}_s) \\ & + C_L \alpha_s \rho_f (\vec{v}_s - \vec{v}_f) \cdot \nabla \vec{v}_f \end{aligned} \tag{4}$$

where τ_s and τ_f represent the stress tensors for both phases respectively,

$$\tau_f = \alpha_f \mu_f (\nabla \vec{v}_f + \nabla \vec{v}_f^{tr}) \tag{5}$$

and

$$\tau_s = \alpha_s \mu_s (\nabla \vec{v}_s + \nabla \vec{v}_s^{tr}) + \alpha_s (\lambda_s - \frac{2}{3} \mu_s) \nabla \vec{v}_s \bar{I} \tag{6}$$

Here, superscript “tr” over velocity vector indicates transpose.

λ_s is solid bulk viscosity given by:

$$\lambda_s = \frac{4}{3} \alpha_s \rho_s d_s g_{o,ss} (1 + e_{ss}) \left\{ \frac{\theta_s}{\pi} \right\}^{\frac{1}{2}} \tag{7}$$

where

$$g_{o,ss} = \left[1 - \left(\frac{\alpha_s}{\alpha_{s,max}} \right)^{\frac{1}{3}} \right]^{-1} \tag{8}$$

The restitution coefficient (e_{ss}) represents the restored KE after the collision of particles. It is generally between 0 and 1.

The shear viscosity of solid particle μ_s is given by:

$$\mu_s = \mu_{s,col} + \mu_{s,kin} + \mu_{s,fr} \tag{9}$$

Solid–liquid momentum transfer coefficient given by:

$$K_{sf} = K_{fs} = \frac{3}{4} \frac{\alpha_s \alpha_f \rho_f}{V_{r,s}^2 d_s} C_D \left(\frac{Re_s}{V_{r,s}} \right) |v_s - v_f| \tag{10}$$

C_D is the given by:

$$C_D = \left[0.63 + 4.8 \left(\frac{Re_s}{V_{r,s}} \right)^{-\frac{1}{2}} \right]^2 \quad (11)$$

Re_s is given by:

$$Re_s = \frac{\rho_f d_s |v_s - v_f|}{\mu_f} \quad (12)$$

Energy equation:

$$u_i \frac{\partial}{\partial x_j} (\theta) = \frac{\partial}{\partial x_j} \left[(1 + \alpha_{t,n}) \frac{\partial}{\partial x_j} (\theta) \right] \quad (13)$$

The eddy diffusivity $\alpha_{t,n}$ is written as follows:

$$\alpha_{t,n} = \frac{v_{t,n}}{Pr_t} \quad (14)$$

The turbulent Prandtl (Pr_t) is taken as 0.71 for air.

Turbulence closure of fluid phase

The k - ε turbulence model is a computational model based on a transport equation for evaluating the velocity range and turbulent range from the turbulent kinetic energy (k) and dissipation rate (ε).

The turbulence quantities for the carrier fluid phase (water) are given by:

$$\overline{\rho u_i' u_j'} = -\mu_t \left(\frac{\partial u_i}{\partial x_j} + \frac{\partial u_j}{\partial x_i} \right) + \frac{2}{3} \rho k \delta_{ij}, \quad (15)$$

Turbulent eddy viscosity is given by,

$$\mu_t = C_\mu \rho \frac{k^2}{\varepsilon} \quad (16)$$

The transport equation for dissipation rate is given by,

$$\frac{\partial}{\partial t} (\rho k) + \frac{\partial}{\partial x_j} (\rho u_j k) = \frac{\partial}{\partial x_j} \left(\frac{\mu_{eff}}{\sigma_k} \frac{\partial k}{\partial x_j} \right) + G - \rho \varepsilon, \quad (17)$$

$$\frac{\partial}{\partial t} (\rho \varepsilon) + \frac{\partial}{\partial x_j} (\rho u_j \varepsilon) = \frac{\partial}{\partial x_j} \left(\frac{\mu_{eff}}{\sigma_\varepsilon} \frac{\partial \varepsilon}{\partial x_j} \right) + C_1 \frac{\varepsilon}{k} G - C_2 \frac{\varepsilon^2}{k} \rho, \quad (18)$$

The constants are given by:

$$C_1 = 1.44, C_2 = 1.92, C_\mu = 0.09, \sigma_k = 1.0, \sigma_\varepsilon = 1.3$$

where,

$$\mu_{eff} = \mu_t + \mu \quad (19)$$

where G is given by,

$$G = \mu_t \left(\frac{\partial u_i}{\partial x_j} + \frac{\partial u_j}{\partial x_i} \right) \frac{\partial u_i}{\partial x_j} \quad (20)$$

Turbulence in the solid phase

As per Tchen's theory, turbulence in the solid phase is predicted for the dispersion of discrete particles in a homogeneous and steady turbulent flow. This model is based on the time scale and characteristics of time theory for predicting the dispersion coefficient, correlation function, and turbulent KE of solid phase dispersion.

The time scale is given by:

$$\tau_{F,sf} = \alpha_s \rho_f K_{sf}^{-1} \left(\frac{\rho_s}{\rho_f} + C_{vm} \right) \quad (21)$$

The characteristic time for turbulent fluctuation due to particle interaction time is given by:

$$\tau_{t,sf} = \tau_{t,f} \left[1 + C_\beta \xi^2 \right]^{-1/2} \quad (22)$$

where

$$\xi = \frac{|\vec{V}_r|}{\sqrt{\frac{2}{3} k_f}} \quad (23)$$

The characteristic time of turbulent eddies is given by:

$$\tau_{t,f} = \frac{2}{3} C_\mu \frac{k_f}{\varepsilon_f} \quad (24)$$

$|\vec{V}_r|$ is the mean relative velocity of solid particles and ambient fluid.

Problem description and boundary conditions

The study of high-speed two-phase slurry jet flow includes the liquid–solid slurry flow that results from the mixing of solid particles and a high-speed carrier fluid. In this study, the phenomena of two-phase flow were used for numerical simulation. Before the computation of two-phase slurry flow, single liquid phase (water) flow was calculated. Liquid phase flow under turbulent conditions was modeled by solving the time average mass continuity equation and general momentum equations employed with the standard k - ε turbulent model as closure. Assuming the slurry flow was in an unsteady state.

In this study, the computational domain consists of an 11-mm pipe with a 2-mm nozzle diameter (D), which is a replication of the geometric model used by Fei Huang et al. [6]. Predicting the jet's velocity structure and the features of the turbulence over its length is the aim. The computational geometry is shown in Fig. 1, where turbulent

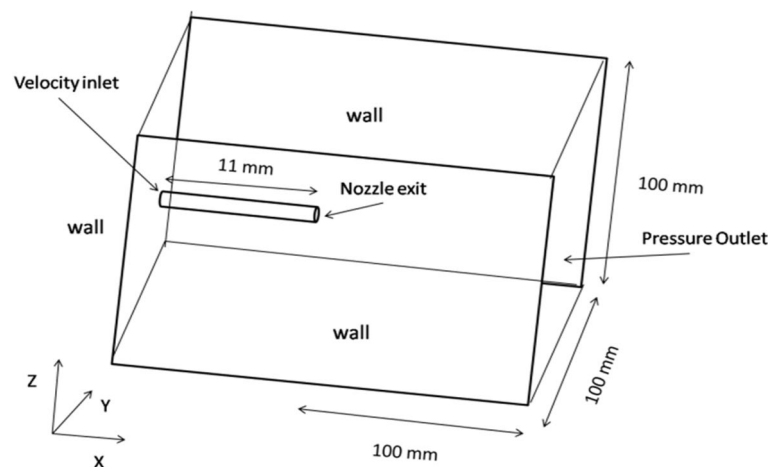


Fig. 1 Computational domain

Table 1 Simulation parameter

Parameter	Details
Abrasive particle material	Al_2O_3 ; (ρ) = 3980 kg/m ³
Particle size (μ m), D_p	25 to 300
Particle concentration (% by volume), C_o	5 to 15
Carrier fluid	Water (a) Density (ρ) = 998.12 kg/m ³ (b) Viscosity (μ) = 0.0010028 kg/m-s $g = 9.81 \text{ m/s}^2$ (-z direction)
Inlet velocity of the jet (m/s), V_o	170 m/s
Inlet condition	Velocity inlet
Outlet condition	Pressure outlet
Turbulence model	k - ϵ model
Multiphase model	Eulerian
Maximum residuals converge criteria	10^{-6}

slurry jet flow is simulated by using a circular nozzle output. Up to 100 mm numerical simulations are run with a view of reproducing the experimental setup used by Fei Huang et al. [6]. With the ANSYS FLUENT 16.0 software, full pipe-flow profiles have been created at the nozzle's exit in this work.

The parameters details are given in Table 1.

The slurry jet's inlet velocity, with water as the primary fluid, is set at 170 m/s. The nozzle is horizontally oriented along the x -axis, and the gravity is in the z -direction.

The mesh distribution is shown in Fig. 2 with the refined structure and the discretization of these equations utilized the finite volume method (FVM) and a power-law differencing scheme. The SIMPLE scheme was implemented for coupling the pressure and velocity terms, while a second-order upwind discretization method was applied to track the behavior of momentum and turbulent factors. Turbulence models employed realizable and standard wall functions within the k - ϵ models. Various

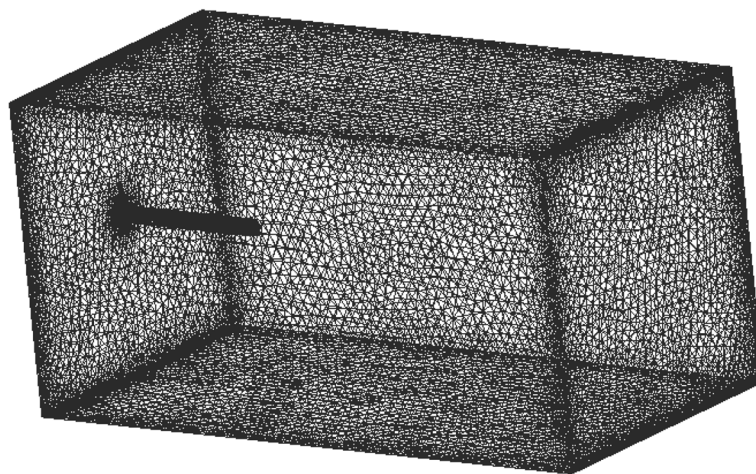


Fig. 2 Mesh distribution

Table 2 Grid independency test results

Type	Node	Element	Mesh quality	Computing time	Mean velocity along the jet centerline axis (m/s)	The experimental data of mean slurry velocity; Fei Huang et al. [6]
Coarse	187,893	78,923	0.32	4 h	72.26	76.25 m/s
Medium	165,892	876,560	0.34	7 h	74.56	76.25 m/s
Fine	145,519	960,303	0.37	9 h	75.26	76.25 m/s

flow parameters were continuously monitored for scaled residuals to achieve solution convergence. In the present computational domain, the base is considered the floor, and pressure outlet conditions are set with a gauge pressure of “0” Pa. Each simulation converged to the criterion of 10^{-6} for successful completion.

Grid structure and independence test

The CFD modeling is performed using the Fluent 16.0 commercial software, and the ICEM module is implemented for mesh generation. Figure 2 shows the mesh arrangement of the computational domain. Table 2 shows the grid information with a different type of mesh and calculation time for simulation.

For the grid independence test, the turbulent slurry flow is examined with coarse, medium, and fine grid types. The jet velocity is 170 m/s for all grid types, and it is worth noting that the increasing grid resolution computational time significantly increases. The maximum difference in the velocity decay rate at the far field is about 3.48% between the coarse structure and the fine structure of the grid. Based on the analysis presented above, a medium structure is chosen for the subsequent numerical simulation investigation.

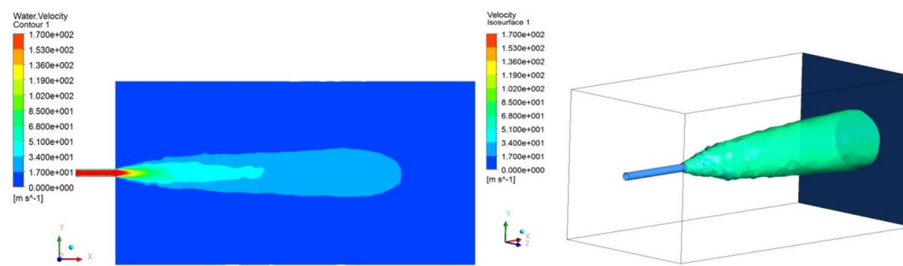


Fig. 3 a Velocity contour for the single-phase fluid jet (water). b Isosurface of the single-phase fluid jet

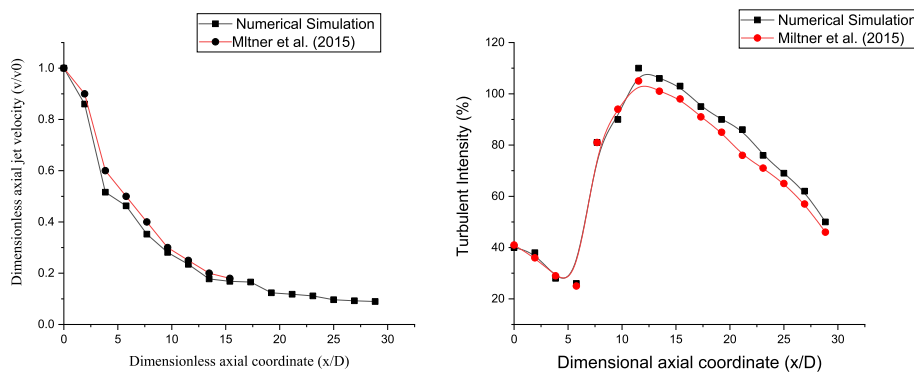


Fig. 4 Comparison of non-dimensional jet velocity (V/V_0) (a) and turbulence intensity (%) (b) against the axial coordinate (x/D)

Results and discussion

Numerical model validation

The velocity contour with isosurface for the single-phase water jet is shown in Fig. 3a, b, spreading jet emerges from the circular nozzle. Initially, the jet enters the computational domain preoccupied with the ambient air. The domain’s outer boundary is set up as the atmospheric pressure-driven pressure release for air that is sinking and flowing sideways. The figure shows the divergence of the jet along its path due to the shear phenomenon that occurred because of the surrounding air resistance at the far field.

The numerical experiments are first compared with the experimental data of Miltner et al. [15], Fig. 4 shows the variation of non-dimensional jet velocity and intensity of turbulent fluctuation water jet along the axial coordinate (x/D). Based on the graph, the numerical simulation for the single-phase jet accurately reflected the experimental findings along the jet axis, with a small variation at the nozzle exit’s far field.

The standard $k-\epsilon$ turbulence model is implemented for simulating the issuing jet, and the divergence along the jet length is increased due to resistance between the outer layer of the jet and the surrounding fluid, which leads to a decrease of jet velocity.

Effect of solid particle concentration on slurry jet structure

Axial velocity

The abrasive particle concentration, jet coherency, and turbulence behavior are some of the elements that have been the focus of much research in recent decades and affect how well a free turbulent slurry jet performs. The core velocity of a high-speed slurry jet and

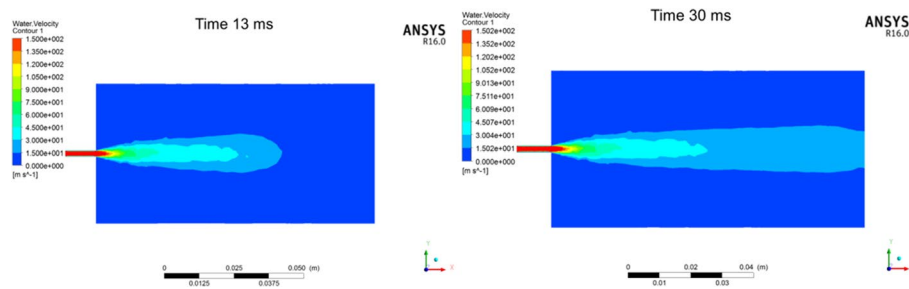


Fig. 5 Velocity contour for the slurry jet with a velocity of $V = 170$ m/s (particle concentration $C_o = 5\%$) emerging from nozzle exit at different time scales

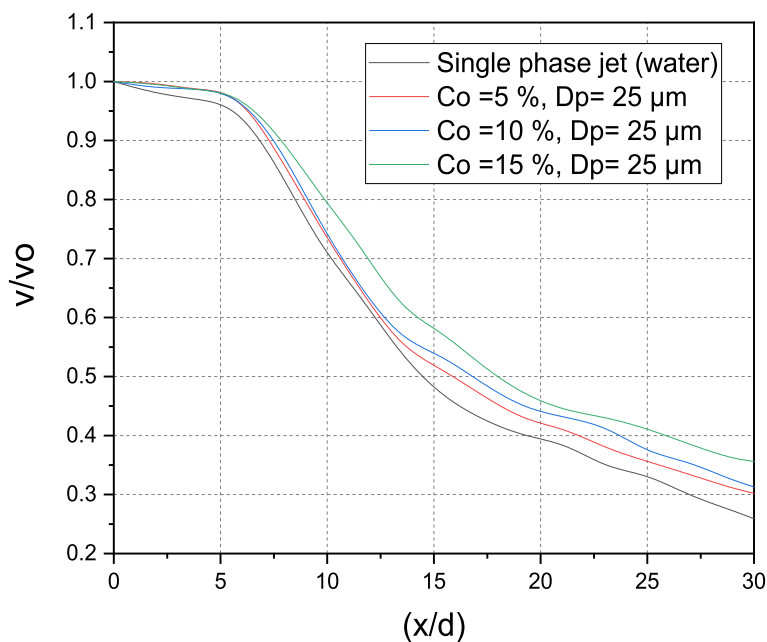


Fig. 6 Variation of non-dimensional velocity profile (V/V_0) along the jet length (x/D) with different particle concentrations (C_o %).

the decay rate of jet issuing from the nozzle exit play a vital role in the jet’s performance. In Fig. 5, the velocity stream of the high-speed slurry jet at various time scales is shown. The velocity contour depicts the spreading of the jet at the far field of the outlet. Because this radial component of velocity increases and the axial velocity of the jet decreases in the case of circular-shaped nozzle geometry, the outer layer of the jet has the least wear resistance from surrounding fluid.

The variation in centerline jet velocity is illustrated in Fig. 5. To comprehensively analyze the flow dynamics, a non-dimensional velocity is employed. The graph illustrates a consistent decrease in the slurry jet velocity along its length. For a particle concentration $C_o = 5\%$, the minimum value of (V/V_0) is observed at 0.3 when x/D equals 30.

Comparing the axial velocity of the slurry jet with a single-phase jet (water), it is noted that the jet with higher particle concentration experiences a 40% lower decay rate than the single-phase water jet. This reduced decay rate is likely attributed to wakes left in the

jet’s path by solid particles. As the number of particles increases, the inter-particle space narrows, causing the wakes to collaborate. This collaboration leads to a decrease in drag, resulting in increased axial velocity due to momentum imbalance.

Figure 6 presents a comparative simulation of a single-phase free turbulent water jet and a slurry jet with 25 μm particle size at various concentrations. The velocity decay rate of the jets with $C_o=5\%$ closely resembles that of single-phase jets (water) for $x/D < 10$. However, for $C_o=10\%$ and 15% , a higher decay rate is observed in the far field of the jet.

The graph shows that for $x/D=15$, the wake-generating method for slurry jets becomes prominent at low abrasive particle concentrations. The centerline velocity for free turbulent slurry jets with a larger particle concentration diverged as compared to the velocity of jets (water) at $x/D=11$. At $x/D=30$, V/V_o decreased to 0.26, whereas for slurry jets with $C_o=5\%$, 10% , and 15% , it is 0.31, 0.32, and 0.37, respectively.

Radial velocity

To give a qualitative measure of particle dispersion of a high-speed slurry jet, the radial profile of the jet is shown in Fig. 7 at the distinct location from the nozzle exit. The graph shows the centerline velocity distribution of the slurry jet against the non-dimensional radial coordinate (y/D) for various slurry concentrations; it can be predicted from the results that the slurry velocity decreases along the jet axis. Figure 7a–c reports the highest velocity for the slurry jet with a high particle concentration, i.e., $C_o=15\%$, while the

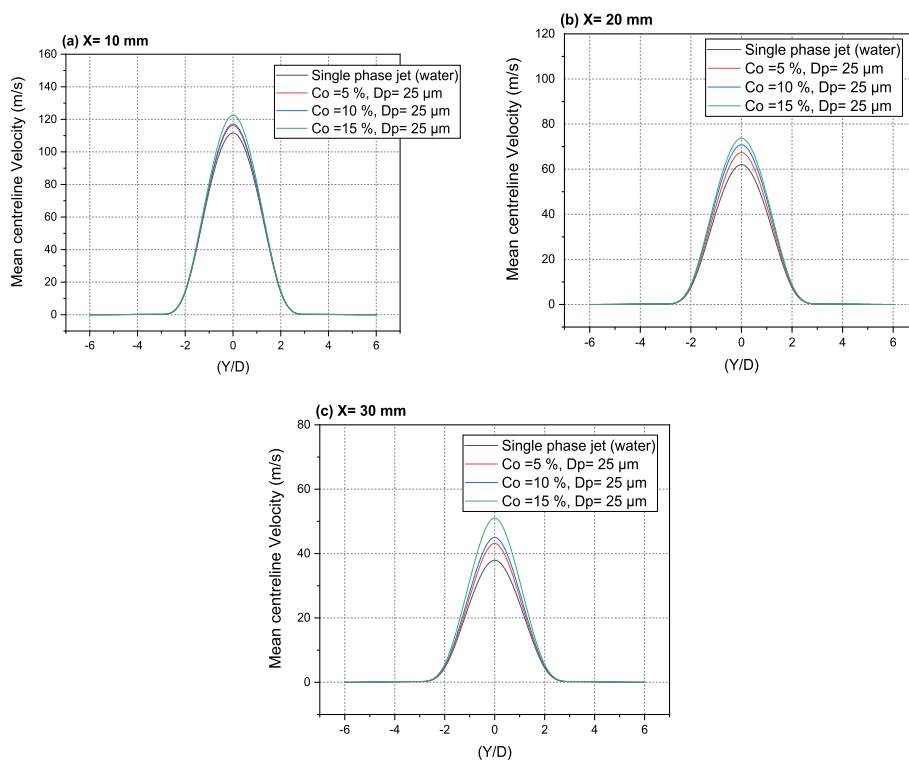


Fig. 7 Variation of mean centerline velocity (m/s) along the radial coordinate at different particle concentrations for various location: $a: x/D=10$, $b: x/D=15$, $c: x/D=30$

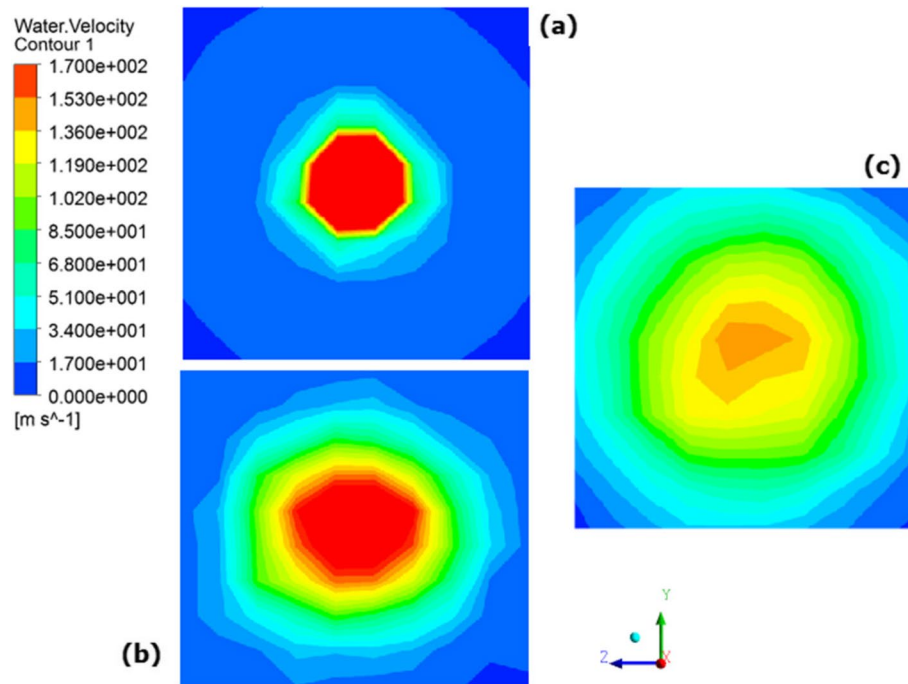


Fig. 8 Circumferential slurry dispersion in jet cross-section. **a** $x/D=10$, **b** $x/D=15$, **c** $x/D=30$

value of the water jet is very near to the smaller particle concentration, while the radial velocity is more accurately predicted by the numerical simulation.

The radial velocities distribution for single phase jet (water) was compared with the slurry jet using computational study. The single-phase jet is utilized for a different sets of numerical experiments along the jet axis, and the numerical results (Fig. 7a–c) for radial component showed similar trends as the experimental observations. The radial component of the slurry jet depends on the axial location. Figure 8 illustrates the contour of the circumferential slurry dispersion in the jet cross-section at a distant location from the nozzle exit (a) $x/D=10$, (b) $x/D=15$, and (c) $x/D=30$ with particle size $25\ \mu\text{m}$ and abrasive particle concentration $C_o=5\%$. It illustrates that the particle size variation has a strong impact on the spreading rate of the jet along the jet. Due to shear phenomena at the far-field area of the jet and resistance from the surrounding fluid, the jet expanded along its length, causing the turbulent slurry jet to diverge. This also reduced the jet's axial component and increased the jet's radial profile. The maximum results of the slurry jet with $C_o=5\%$, 10% , and 15% at $x/D=10$ is 0.0454 , 0.064 , and 0.109 times higher than the single-phase jet respectively. A similar trend is seen for $x/D=15$ and $x/D=30$.

Turbulence characteristics

This section of work deals with the investigation of turbulence characteristics for various particle concentrations of turbulent slurry jets at various dimensionless coordinates (x/D). Numerous experimental experiments have demonstrated that the second phase's interaction with the jet flow systems causes variation in the turbulence level (i.e., abrasive particles). Turbulence modulation is the term used in literature to describe the variation in turbulence strength caused by solid particles. It was discovered that for the

correlation of turbulence modulations, the ratio of abrasive particle size to the most energetic eddy particle.

It was expanded by Azimi et al. [3], who also gave logarithmic formulae for forecasting variations in the strength of the turbulence. According to experimental models of turbulent water jet flow, the amount of turbulence was significantly lower than in the single-phase turbulent jets. According to reports, the high-speed slurry jet had turbulence intensity drops between 30 and 70%.

The turbulence kinetic energy of slurry issuing from the nozzle is clearly shown in Fig. 9a: the disturbance of the jet against the surrounding air due to the shear resistance offered and velocity transfer between the abrasive particle and ambient air.

Figure 9b shows the comparative analysis of turbulence intensity (%) of the slurry jets and the corresponding single-phase water jets. It shows that at $x/D=30$, the average turbulence intensity along the axis jet was registered around 39% below that of single-phase turbulent jets with water as the primary fluid. It shows that the instantaneous fluctuations of the slurry jet at different particle concentrations decrease as the particle concentration increases along the jet axis.

Effect of particle size on slurry jet structure

In this section, the flow properties such as axial velocity, radial velocity, and turbulent characteristics were studied on the verge of particle size variation. The numerical simulation results indicate a clear impact on flow behavior due to variations in particle size and initial concentration of the slurry jets. Figure 10 shows the graphical variation of dimensional velocity along the jet axis at different particle sizes. It can be predicted that the decay rate keeps on elevating at the far field ($x/D=30$) by increasing the size of the abrasive particle; this may be due to the bulk density of slurry increases which leads to lower resistance and shear phenomenon at the far field of the jet.

At $x/D=10$, the maximum velocity of jet with particle size of 25 μm , 75 μm , 150 μm , and 300 μm are respectively 1.13, 1.18, and 1.24 times the single-phase jet velocity. The axial velocity of the slurry jet at particle size 25 μm was around 4% greater at $x/D=10$ than the single-phase jets. At 75 μm , 150 μm , and 300 μm particle size, the axial

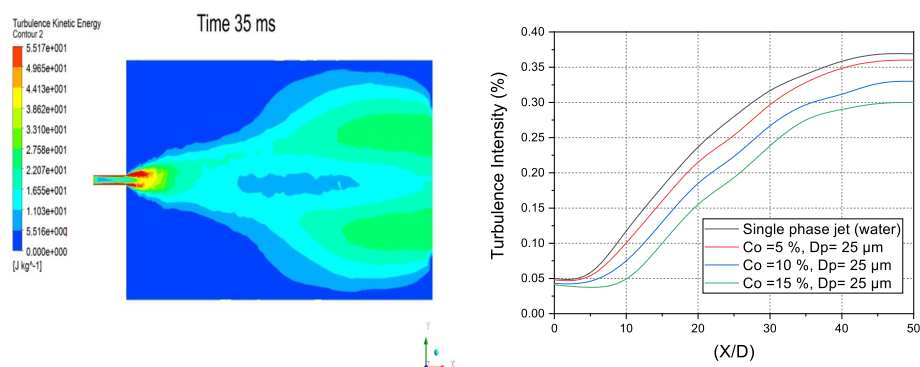


Fig. 9 a Turbulence kinetic energy contour for particle size 25 μm , particle concentration $C_o = 5\%$ with inlet velocity 170 m/s. b Variation of Turbulence intensity of slurry with (x/D) at different particle concentrations (C_o %)

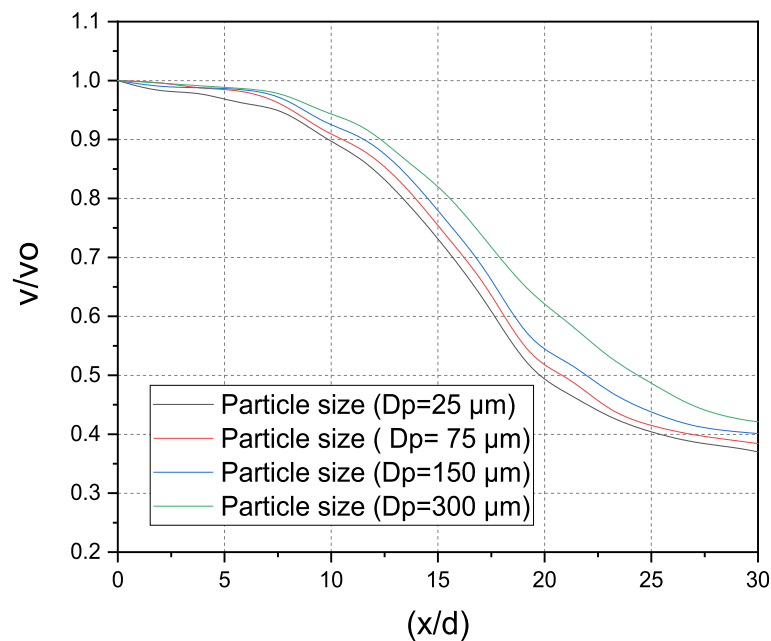


Fig. 10 Variation of non-dimensional slurry velocity profile (V/V_0) along the jet length (x/D) with different particle sizes (D_p) and different concentrations

velocities were, respectively, 11.51, 14.26, and 23.45% higher than single-phase turbulent jets. Particle velocity decays gradually at a lower rate than the single-phase jet at a far field distance ($x/D=30$). As a result, the slurry velocities with particle sizes 25 μm , 75 μm , 150 μm , and 300 μm were 4%, 25%, and 34% greater than those of single-phase turbulent free jets, respectively. Due to the dependency of contact forces on particle size, the velocity of the slurry jet varies accordingly. However, this variation is less pronounced compared to that observed in turbulent slurry jets.

In Fig. 11, the estimated radial velocities of a slurry jet with various particle sizes are displayed. It shows that the radial component of slurry velocity is influenced predominantly by the increasing particle size. When the particle size grows, the value of radial velocity increases far from the jet nozzle ($x/D=30$). Due to this, the interparticle spacing is the cause of the higher value of radial velocity. The distance between the larger particles will be high at the same particle concentration, or 5% of the total volume, which allows for the formation of larger eddies.

The numerical simulation results for radial velocity were compared with observations by Miltner et al. [15] using a single-phase water turbulent jet. The radial velocity of the scattered phase in their experimental observations followed the same trend as the computational results reported, with a small divergence.

In certain situations, the divergence of the jet as represented by the normalized slurry jet flow emanating from the nozzle was not constant. Particles with larger-sized jets have a faster-spreading rate in these ranges of particle sizes. For slurry jets with 25 μm particle sizes, the normalized slurry jet flow was calculated to be 0.065. For jets with 75, 150, and 300 μm , the obtained spreading rates were 0.115, 0.18, and 0.22, respectively. The high potential energy of larger particles converted to kinetic energy through the jet may be the cause of the larger particle jets observed and faster-spreading rates. More particle

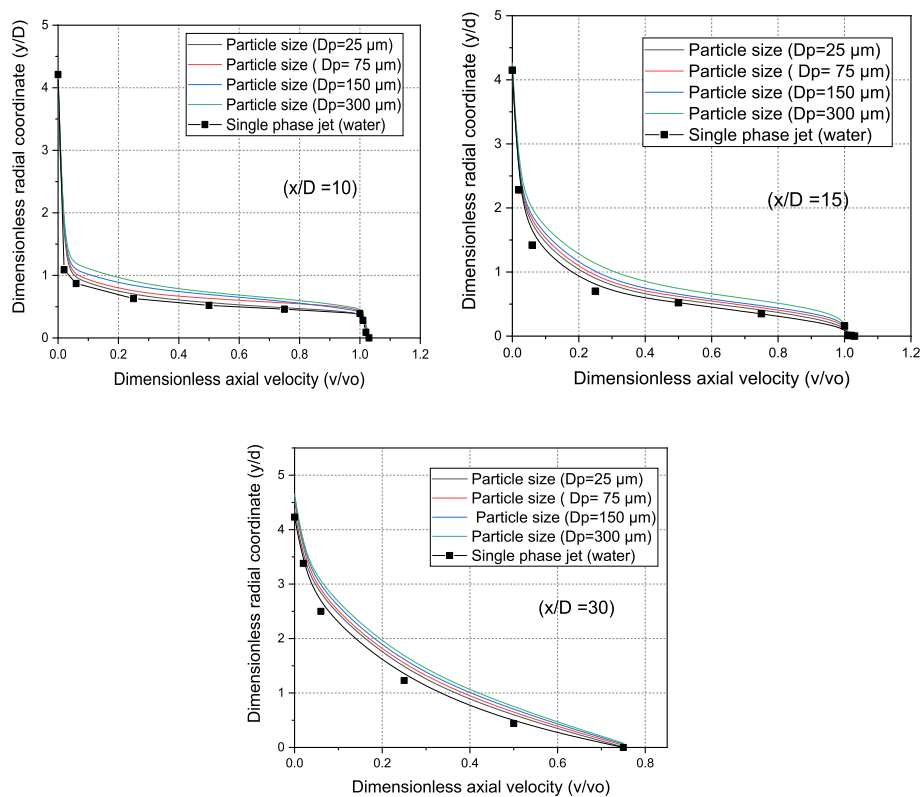


Fig. 11 Variation of non-dimensional axial velocity (V/V_0) of slurry jet on the radial coordinate (y/D) at a different location from nozzle exit (x/D)

fluctuations caused by higher kinetic energy result in increased spreading rate and particle dispersion.

Figure 12 depicts the turbulent fluctuation of the slurry jet at different particle sizes. It is significant from the graph that less dissipation of the jet was observed for larger particles. The variation of turbulence fluctuation of jets with 25- μm particles was higher by 4.39%, 5.21%, and 13.12%, respectively, than that of the jets with 75- μm , 150- μm , and 300- μm particles. For a portion of their existence, fine particles mostly follow eddies with turbulence, and the drag force that propels particle movement transfers the eddy's energy to the particles. As a result, continuous-phase energy is dissipated by small particles more quickly than by large particles. The graphic shows the results of the amount of turbulence. The peak value of turbulence decreases at the far field at all particle sizes due to the large eddy formation.

Larger particles produce a bigger fluctuation in turbulence than smaller ones close to the jet nozzle. The turbulence intensity for 25 μm particles at $x/D = 10$ was 2.36, 4.25, and 8.3% less than that for 75, 150, and 300 μm particles, respectively. Large particles have more inertia than smaller ones and follow the turbulence fluctuation more quickly even when they have the same continuous-phase kinetic energy. This may be the cause of the small particles' reduced turbulent intensity when compared to the large particles. Although reducing the radial coordinate (y/D) always increases the value of turbulence intensity, the maximum value varies with the particle size

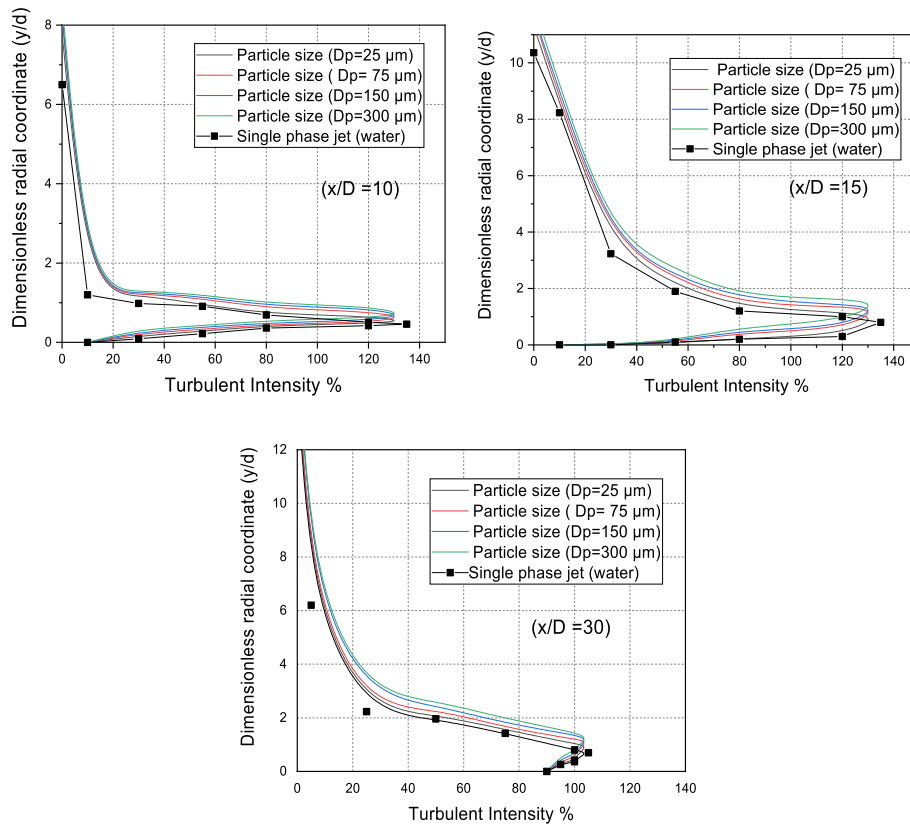


Fig. 12 Variation of turbulent intensity (%) of slurry jet on the radial coordinate (y/D)

variation. Peak turbulent intensity was reached for turbulent slurry jets at $x/D = 10$ with 25- μm particles at 0.54; however, this value was 0.63, 0.68, and 0.72 for slurry jets with 75- μm , 150- μm , and 300- μm particles. This (Fig. 12b, c) shows how the turbulence fluctuation changes as the radial distance increases, and the jet moves away from the centerline axis. At $x/D = 30$, slurry jets with 150- μm particles reduce turbulent intensity by 7.2%, while those with 75- μm particles reduce turbulent intensity by 14.32%.

Thermal analysis of the free turbulent slurry jet

The thermal characteristics of the jet are performed along the jet axis, and the temperature profile is observed for different particle concentrations. The inlet section temperature and outlet section temperature of the jet is kept constant at 300 K. The slurry jet impinges on the surrounding ambient fluid maintained at 300 K temperature, and the surface of the computational domain wall is maintained at 330 K temperature.

The numerical results are first validated with the experimental results performed by Holland and Liburdy [10] with the same boundary conditions and maintaining the adiabatic surface of the wall. Figure 13 shows the non-dimensional temperature profile variation at different non-dimensional axial coordinates (x/D) = 10, 15, and 30. The present numerical simulations are well accompanied by the literature results with minimum errors of divergence.

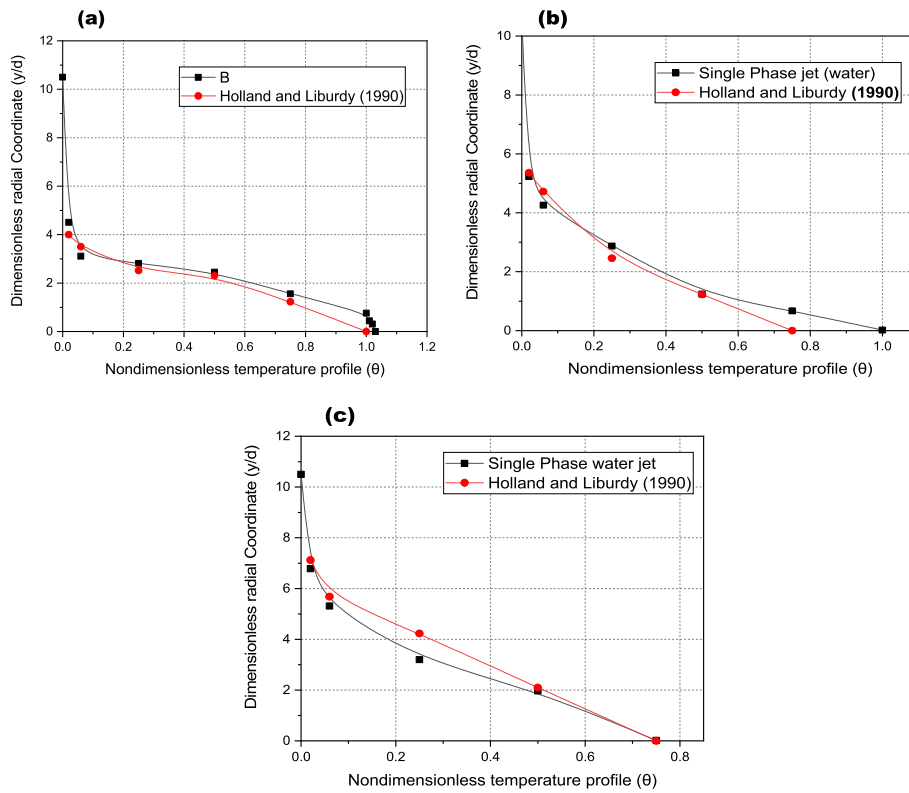


Fig. 13 Temperature profile distribution with (y/D) at the various locations: **a**: $x/D = 10$, **b**: $x/D = 15$, and **c**: $x/D = 30$

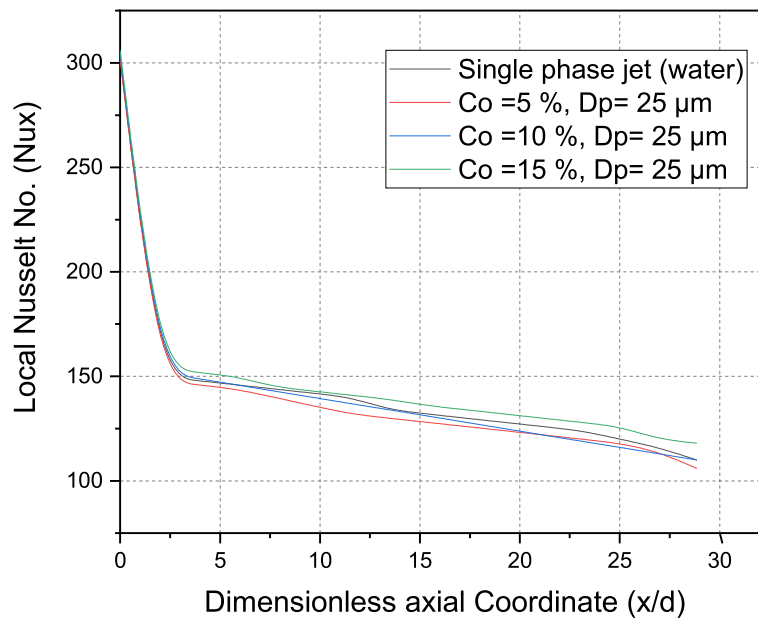


Fig. 14 Local Nusselt number distribution for different particle concentrations (C_o)

Local Nusselt number

The local Nusselt number (Nu_x) is evaluated as follows:

$$Nu_x = \frac{Q \text{ Pr Re}}{\rho C_p v (T_w - T_\infty)} \tag{25}$$

From the above equation, the Nusselt number is calculated along the jet axis. Figure 14 shows the maximum variation of Nu_x at the inlet of the jet, and as the axial velocity decreases, the local Nusselt number also decreases.

The graph depicts the maximum values of local Nusselt number (Nu_x) evaluated at the start of the jet for all the considered cases; their values are 297, 299, 301, and 303 for single-phase water jet, $C_o=5\%$, $C_o=10\%$, and $C_o=15\%$ particle concentrations respectively. In Fig. 14, it is visible that the particle concentration can affect heat transfer. Comparing the results of local Nusselt numbers with different particle concentrations with single-phase water jet, it is found that the maximum variation is reported between $x/D=10$ to 15 with 2.7%, 9.35%, and 15.36% variation at $C_o=5\%$, $C_o=10\%$, and $C_o=15\%$ particle concentrations respectively. This is due to the overlapping of the slurry jet with the ambient air, which leads to an increase in the self-similarity of the jet at the far field.

Figure 15 depicts a comparison of temperature distribution of a free turbulent slurry jet with single-phase water jet for different particle sizes (D_p), i.e., 25 μm , 75 μm , 150 μm , and 300 μm along the jet length. The temperature profile shows clear similarity with the single-phase jet (water) at the near field of the jet, but at the far field, the jet shows a noticeable variation in temperature distribution. For small particle sizes, there is no significant influence on the thermal characteristics of the jet. However, with a gradual increase in the particle size beyond 75 μm , the heat transfer

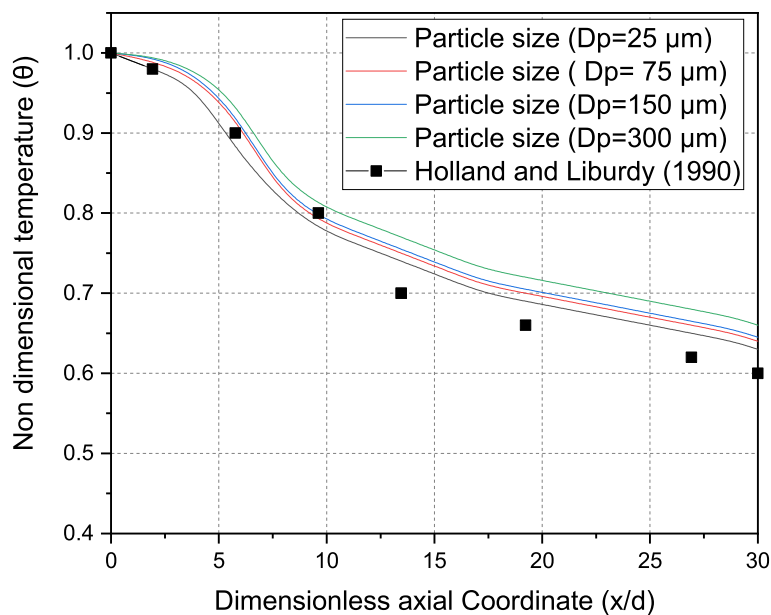


Fig. 15 Non-dimensional temperature profile distribution along the jet axis for different particle sizes (D_p)

rate increased drastically with 5.6%, 8.9%, and 11.54% for 75 μm , 150 μm , and 300 μm particle sizes respectively. This enhancement is due to the increased thermal conductivity of particles in the water which induces the thermal diffusion effect and increases the heat transfer rates.

Conclusions

We conducted the CFD simulation for free turbulent slurry flow to properly study the flow dynamics of the jet and the thermal behavior of the turbulent slurry jet. Results show that the parametric CFD is an efficient tool for future engineering applications. The following observations were made during the numerical investigation:

- (i) Numerical results show that the axial velocity of the slurry jet decays at a slower when compared to a single-phase jet (water). It was observed that for axial length $x/D=15$, the wake-generating method for slurry jets becomes prominent at low abrasive particle concentrations. The centerline velocity for free turbulent slurry jets with a larger particle concentration shows maximum divergence related to the single-phase free turbulent water jets velocity at $x/D=11$. At the far field of the jet says $x/D=30$, V/V_o decreased to 0.26, whereas for slurry jets with $C_o=5\%$, 10%, and 15%, it is 0.31, 0.32, and 0.37, respectively.
- (ii) The jet diverges radially due to the resistance from the surrounding fluid and shear phenomena at the far-field region of the jet due to which the divergence of the turbulent slurry jet is observed, and it decreases the axial component of the jet and the radial profile of the jet enlarged. The maximum velocity of the slurry jet with $C_o=5\%$, 10%, and 15% at $x/D=10$ is 0.0454, 0.064, and 0.109 times higher than the single-phase jet respectively. A similar trend is seen for $x/D=15$ and $x/D=30$. The comparison between the single-phase water jet and slurry jet for turbulence intensity along the axis shows a decrement of 39% at ($x/D=30$).
- (iii) The divergence of the slurry jet is prominently related to the variation of abrasive particle size; smaller particle size has less inertia during the propagation of the jet, while the divergence of the jet with medium-sized particles and large-sized particles prominently depends on the collaborative mechanism of inertia and centrifugal phenomenon. As particle size grows, the slurry jet's axial velocity decay rate increases along the jet. The calculated maximum velocities for particle sizes of 25 μm , 75 μm , 150 μm , and 300 μm were, respectively, 1.13, 1.18, and 1.24 times the water jet at the near field of the jet, i.e., $x/D=10$. For a portion of their existence, fine particles frequently undergo turbulent eddies, and the drag force that propels particle movement transfers the eddy's energy to the particles. As a result, continuous-phase energy is dissipated by small particles more quickly than by large particles. The graphic shows the results of the amount of turbulence. The peak value of turbulence decreases at the far field at all particle sizes due to the large eddy formation.
- (iv) Comparison of non-dimensional temperature profiles with the previous literature work for different axial coordinates (x/D) = 10, 15, and 30. The numerical simulations are well accompanied by the literature results of Holland and Liburdy [10] with minimum errors of divergence. Comparing the results of local Nusselt numbers with different particle concentrations with single phase jet, it is shown that the maximum variation is reported between $x/D=10$ to 15 with 2.7%, 9.35%,

and 15.36% variation at $C_o = 5\%$, $C_o = 10\%$, and $C_o = 15\%$ particle concentrations respectively. For small particle size, there is no significant influence on the thermal characteristics of the jet. However, with a gradual increase in the particle size beyond $75 \mu\text{m}$, the heat transfer rate increased drastically with 5.6, 8.9, and 11.54% for $75 \mu\text{m}$, $150 \mu\text{m}$, and $300 \mu\text{m}$ particle sizes respectively.

The CFD simulation of turbulent slurry jet dynamics reveals slower axial velocity decay compared to single-phase jets. Radial divergence is prominent, influenced by abrasive particle size. Fine particles dissipate energy more quickly due to turbulent eddies, affecting jet turbulence. Thermal characteristics show significant heat transfer rate increases with larger particle sizes. Overall, the study underscores the impact of particle size on flow and thermal behavior in turbulent slurry jets.

Abbreviations

V	Inlet velocity of Jet (m/s)
V_o	Instant velocity of jet along jet axis (m/s)
D	Inner diameter of the nozzle (mm)
C_o	Particle concentration (% by volume)
D_p	Solid particle size (μm)
\vec{i}	Identity tensor
d_s	Particle diameter
$g_{o,ss}$	Radial distribution function
$a_{s,max}$	Static settled concentration
θ_s	Granular temperature
e_{ss}	Restitution coefficient
μ_s and μ_f	Shear viscosity of the solid particle and fluid
$\mu_{s,col}$, $\mu_{s,kin}$ and $\mu_{s,fr}$	Collisional, kinetic, and frictional viscosity respectively
C_D	Drag coefficient
Re_s	Relative Reynolds number
ν_t	Turbulent eddy viscosity
ρ	Density (kg/m^3)
C_{b1}, C_{b2}	Model constants
C_{w1}, C_{w2}	Model constants
\bar{s}	Turbulence production
S	Modulus of strain tensor
Ω	Rotational tensor
β	Thermal expansion coefficient
ε	Dissipation rate of Turbulence
p_k	Kinetic energy production factor
β^*	Constant
F_1, F_2	Constant
C_μ	Constant
k	Kinetic energy (turbulence)
μ_t	Viscosity (turbulence)
C_2, C_1	Model constant
η, η_0	Constant
Nu_x	Local Nusselt number
Q	Average heat flux
C_p	Specific heat at constant pressure, $\text{J}/\text{kg}/\text{K}$
Θ	Non-dimensional temperature, $\frac{T - T_\infty}{T_0 - T_\infty}$
T_0	Jet Inlet temperature, K
T_∞	Surrounding temperature, K
T	Instantaneous temperature, K

Acknowledgements

The authors are thankful to NIT Raipur (CG) for providing computational lab and library resources.

Authors' contributions

All authors contributed to the conception and design of the study. All authors critically revised the manuscript, provided intellectual input, and approved the final version for submission.

Funding

The submitted research paper did not receive any funding.

Availability of data and materials

Not applicable.

Declarations**Competing interests**

The authors declare that they have no competing interests.

Received: 29 December 2023 Accepted: 2 September 2024

Published online: 10 September 2024

References

1. Azimi AH, Qian Y, Zhu DZ, Rajaratnam N (2015) An experimental study of circular sand–water wall jets. *Int J Multiphase Flow* 74:34–44
2. Azimi AH, Zhu DZ, Rajaratnam N (2011) Effect of particle size on the characteristics of sand jet in water. *J Eng Mech* 137(12):822–834
3. Azimi AH, Zhu DZ, Rajaratnam N (2012) Experimental study of sand jet front in water. *Int J Multiphase Flow* 40:19–37
4. Li D, Fan J, Luo K, Cen K (2011) Direct numerical simulation of a particle-laden low Reynolds number turbulent round jet. *Flow* 37(6):539–554
5. Fan J, Zhang L, Zhao H, Cen K (1990) Particle concentration and particle size measurements in a particle laden turbulent free jet. *Exp Fluids* 9:320–322
6. Huang Fei, Mi Jianyu, Li Dan, Wang Rongrong (2020) Impinging performance of high-pressure water jets emitting from different nozzle orifice shapes, Hindawi. *Geofluids* 2020:14
7. Liu H, Wang J, Kelson N, Brown RJ (2004) A study of abrasive waterjet characteristics by CFD simulation. *J Mater Process Technol* 153–154:488–493
8. Sheen HJ, Jou BH, Lee YT (1994) Effect of particle size on a two-phase turbulent jet. *Science* 8:315–327
9. Hall N, Elenany M, Zhu DZ, Rajaratnam N (2010) Experimental study of sand and slurry jets in water. *J Hydraul Eng* 136:727–738
10. Holland JT, Liburdy JA (1990) Measurements of the thermal characteristics of a heated offset jets. *Int J Heat Mass Transf* 33(1):69–78
11. Fan JM, Fan CM, Wang J (2011) Flow dynamic simulation of micro abrasive water jet. *Solid State Phenom* 175:171–176
12. Gopaliya MK, Kaushal DR (2016) Modeling of sand-water slurry flow through horizontal pipe using CFD. *J Hydrol Hydromech* 64:261–272
13. Matthias Eng and Anders Rasmuson (2014) Measurement of continuous phase velocities in a confined solid-liquid jet using LDV. *Chem Eng Commun* 201:1497–1513
14. Melentjeva R, Fang F (2019) Theoretical study on particle velocity in micro-abrasive jet machining. *Powder Technol* 344:121–132
15. Miltner M, Jordan C, Harasek M (2015) CFD simulation of straight and slightly swirling turbulent free jets using different RANS-turbulence models. *App Thermal Engg* 89:1117–1126
16. Sharma NK, Dewangan SK, Gupta PK (2023) Numerical simulation of three-dimensional circular free turbulent jet flow using different Reynolds average Navier-Stokes turbulence models. *Comput Therm Sci Int J* 15(3):79–97
17. Nguyen T, Shanmugam DK, Wang J (2008) Effect of liquid properties on the stability of an abrasive waterjet. *Int J Mach Tools Manuf* 48:1138–1147
18. Liu P, Lam KM (2015) Simultaneous PIV measurements of fluid and particle velocity fields of a sediment-laden buoyant jet. *Journal of Hydro-environment Research* 9(2):314–323
19. Rao R, Anil K (2019) Heat transfer distribution of impinging methane-air premixed flame jets. Ph.D. diss., National Institute of Technology Karnataka, Surathkal.
20. Rehman MM, Qu ZG, Fu RP, Xu HT (2017) Numerical study on free-surface jet impingement cooling with nano encapsulated phase-change material slurry and nanofluid. *Int J Heat Mass Transf* 109:312–325
21. Saleh SN, Saaed O, Skydnenko M (2020) CFD assessment of jet flow behavior in an alternative design of a spray dryer chamber. *Adv Des Simul Manufact II*:863–870
22. Sarkar A, Nitin N, Karwe MV, Singh RP (2004) Fluid flow and heat transfer in air jet impingement in food processing. *J Food Sci* 69:4
23. Karimi S, Mansouri A, Shirazi SA, McLaury BS (2017) Experimental investigation on the influence of particle size in a submerged slurry jet on erosion rates and patterns. In *Fluids Engineering Division Summer Meeting* (Vol. 58066, p. V01CT15A007). American Society of Mechanical Engineers.
24. Wen-xin HUAI, Wan-yun XUE, Zhong-dong QIAN (2013) Numerical simulation of slurry jets using mixture model. *Water Sci Eng* 6(1):78–90
25. Zhou X, Sun Z, Durst F, Brenner G (1999) Numerical simulation of turbulent jet flow and combustion. *Computers and Mathematics with Application* 38:179–191

Publisher's Note

Springer Nature remains neutral with regard to jurisdictional claims in published maps and institutional affiliations.